

The effects of temperature and vacancy defect on the severity of the SLGS becoming anisotropic

Vahid Tahouneh*, Mohammad Hasan Naei and Mahmoud Mosavi Mashhadi

School of Mechanical Engineering, College of Engineering, University of Tehran, Tehran, Iran

(Received August 29, 2018, Revised October 24, 2018, Accepted November 15, 2018)

Abstract. Geometric imperfections may be created during the production process or setting borders of single-layer graphene sheets (SLGSs). Vacancy defects are an instance of geometric imperfection, so investigating the effect of these vacancies on the mechanical properties of single-layer graphene is extremely important. Since very few studies have been conducted on the structure of imperfect graphene (with the vacancy defect) as an anisotropic structure, further study of this defective structure seems imperative. Due to the vacancy defects and for the proper assessment of mechanical properties, the graphene structure should be considered anisotropic in certain states. The present study investigates the effects of site and size of vacancy defects on the mechanical properties of graphene as an anisotropic structure using the Lekhnitskii interaction coefficients and Molecular Dynamic approach. The effect of temperature on the severity of the SLGS becoming anisotropic is also investigated in this study. The results reveal that the amount of temperature has a big effect on the severity of the structure getting anisotropic even for a graphene without any defects. The effect of aspect ratio, temperature and also size and site of vacancy defects on the material properties of the graphene are studied in this research work. According to the present study, using material properties of flawless graphene for imperfect structure can lead to inaccurate results.

Keywords: molecular dynamic; graphene; vacancy defect; lekhnitskii coefficients; anisotropic materials; temperature effects

1. Introduction

Advances in nanoscience have led to the emergence of an extensive range of nanoscale systems and equipment such as nano-electromechanical systems. Due to their unique mechanical, electronic, optical and thermal properties, carbon nanotubes, graphene ribbons and graphene sheets currently have a wide range of applications in these systems. The analysis and assessment of these structures are therefore very important. As a nanostructure, graphene contains a layer of covalently-bonded carbon atoms in a honeycomb structure (Iijima 1991). Graphene has attracted the particular attention of researchers due to its special mechanical, electrical and thermal properties and also its fairly low production cost (Dai 2002, Navarro *et al.* 2007, Lee *et al.* 2008, Yakobson *et al.* 1996, Stankovich *et al.* 2006). A variety of theoretical methods have been used to examine the mechanical and elastic properties of an ideal and flawless single-layer graphene sheet, including density functional theory (DFT), quantum mechanics, molecular dynamic simulation and continuous medium mechanics. Liu *et al.* (2007) found Young's modulus as 1.05 TPa for single-layer graphene using the density functional technique. Jiang *et al.* (2009) investigated Young's modulus for different sizes of single-layer graphene at different temperatures

using molecular dynamics. Shen *et al.* (2010) examined Young's and shear moduli of nanoscale structures at different temperatures. The analysis of failure and ultimate strength of single-layer graphene sheets was carried out by Ni *et al.* (2010), who showed that these nanostructures are much stronger in armchair alignment than zigzag alignment. Tsai and Tu (2010) examined the mechanical properties of graphene by molecular dynamics. The main problems with atomic models include time-consuming calculations and the subsequent limitation in the dimensions of molecular and atomic structures. Great efforts have therefore been made in recent years to develop nanoscale theories of continuous medium mechanics. To this end, Reddy *et al.* (2006) found Young's modulus as 0.669 TPa for single-layer graphene using continuous medium mechanics. Sakhaee-Pour (2009) and Georgantzinos *et al.* (2010) found Young's modulus values as 1.025 TPa and 1.367 TPa respectively, using the finite element technique, in which the atomic bonds were modelled as truss, beam or spring. Graphene sheets appear as wrinkled when in equilibrium. These wrinkles can have a height of 7 Å. Moreover, defects called the ridge defect also appear on graphene sheets due to shearing strain (Udupa and Martini 2011). Bu *et al.* (2009) used molecular dynamic simulation to assess the mechanical properties of armchair-structured graphene nanoribbons at 300 K. This simulation indicated the presence of 0.88-nm-high bulges and wrinkles in the nanoribbons equivalent to approximately a 5%-strain on the nanoribbon. Kvashnin *et al.* (2010) investigated the properties of circular graphene for various radii and also the effect of different densities of vacancy defects on the

*Corresponding author, Ph.D. Student,
E-mail: vahid.th1982@gmail.com;
vahid.tahouneh@ut.ac.ir

mechanical properties of single-layer graphene sheet. The Stone-Wales defect in graphene and other substances with a covalence bond configuration of the geometric type sp^2 were investigated by Ma *et al.* (2009). Tahouneh *et al.* (2016) studied the effect of fiber reinforced CNT arrays on the material properties of nanocomposites. Tornabene *et al.* (2018) studied free vibration of laminated nanocomposite plates and shells using first-order shear deformation theory and the Generalized Differential Quadrature (GDQ) method. Each layer of the laminate was modelled as a three-phase composite. A survey of several methods under the heading of strong formulation finite element method (SFEM) was presented by Tornabene *et al.* (2015). These approaches were distinguished from classical one, termed weak formulation finite element method (WFEM). Soleimani *et al.* (2017) investigated the postbuckling characteristics of single layered graphene sheets (SLGSs) using Nonlocal elasticity theory and von-Karman nonlinear model in combination with the isogeometric analysis (IGA). Jalali *et al.* (2016) investigated the influence of out-of-plane defects on vibrational analysis of single layered graphene sheets. Marin (2008) proved the existence and uniqueness of the generalized solutions for the boundary value problems in elasticity of initially stressed bodies with voids (porous materials). Marin and Öchsner (2017) studied the mixed initial boundary value problem for a dipolar body in the context of the thermoelastic theory proposed by Green and Naghdi. For the solutions of this problem, Marin and Öchsner (2017) proved a result of Hölder's-type stability on the supply terms. Marin (2016) formulated a heat-flux theory for taking into account a new set of state variables including the heat-flux vector and an evolution equation for it. Marin (1997) proved that the Cesaro means of the kinetic and strain energies of a solution with finite energy became asymptotically equal as time tended to infinity. The same author (Marin 2010) considered a right cylinder composed of a physically dipolar thermoelastic material for which one plane end was subjected to an excitation which was harmonic in time. He obtained a spatial decay estimate, similar to that of Saint-Venant type. Zhang *et al.* (2009) used the governing equations and simulation to indicate that the gas-identification property of chemical sensors increases significantly in graphene with the vacancy defect compared to defect-free graphene. Kumar and Srivastava (2016) investigated the effective elastic properties of CNT- and graphene-based nanocomposites using 3-D nanoscale representative volume element (RVE) based on continuum mechanics using finite element method (FEM). Moradi-Dastjerdi and Payganeh (2017a) studied thermoelastic dynamic behavior of functionally graded carbon nanotube reinforced composite (FG-CNTRC) cylinders subjected to mechanical pressure loads, uniform temperature environment or thermal gradient loads by a mesh-free method. Moradi-Dastjerdi and Momeni-Khabisi (2016) investigated free vibration, forced vibration, resonance and stress wave propagation behavior in nanocomposite plates reinforced by wavy carbon nanotube (CNT). Moradi-Dastjerdi and Payganeh (2017b) considered transient heat transfer analysis of functionally graded (FG) carbon nanotube reinforced nanocomposite (CNTRC) cylinders

with various essential and natural boundary conditions. Tahouneh (2017) studied effects of CNTs waviness and aspect ratio on vibrational response of FG-sector plate using GDQ method. Tahouneh (2017) investigated free vibration analysis of continuously graded carbon nanotube-reinforced (CGCNTR) rectangular plates resting on two-parameter elastic foundations. The volume fractions of oriented, straight single-walled carbon nanotubes (SWCNTs) were assumed to be graded in the thickness direction. Allahkarami *et al.* (2018) examined the in-plane and out-of-plane forced vibration of a curved nanocomposite microbeam. The same authors (2017) investigated the magneto-thermo-mechanical vibration and damping of a viscoelastic functionally graded-carbon nanotubes (FG-CNTs)-reinforced curved microbeam based on Timoshenko beam and strain gradient theories. Sun *et al.* (2014) also studied the effect of vacancy defects on the ultimate strength of graphene sheets. In another study (Sun *et al.* 2015), molecular dynamic modelling was used to investigate the effect of defects on the unique properties of graphene while considering graphene an anisotropic structure. This research work revealed that graphene properties are totally dependent on angular orientation. The authors showed that the mechanical properties of graphene sheets are least sensitive to vacancy defects at the angle of 15 degree. Wu *et al.* (2015) found dynamic properties and relaxation time for a variety of graphene groups with vacancy defects using molecular dynamic simulation in Large-scale Atomic/Molecular Massively Parallel Simulator (LAMMPS). They showed that the maximum dynamic displacements of graphene increase with the number and size of vacancy defects. Based on theories relating to graphene molecular bonds, Xie *et al.* (2014) studied the effect of single- and double-vacancy defects on the photonic properties and thermal conductivity of graphene with defects and showed that the type of these defects has a significant effect on the photo and thermal conductivity of graphene. Neek-Amal and Peeters (2010) performed the MD simulation of nano-indentation of circular graphene sheets similar to the experiments of Lee *et al.* (2008). Utilizing quantum mechanics, Yanovsky *et al.* (2009) obtained mechanical properties of graphene sheets. None of the cited studies have investigated the properties of imperfect graphene with an anisotropic structure. Given the existing articles and information related to the authors of this research work, no articles have yet been published for investigating the effect of vacancy defects on the material properties of single-layer graphene as an anisotropic structure using Lekhnitskii interaction coefficients and the molecular dynamic method. Other researchers have addressed the vibrational and stress analysis of graphene structures with vacancy or Stone-Wales defects. It is worth noting that, despite assuming vacancies in fairly simple shapes at different analytical and semi-analytical solutions, these researchers have still used the mechanical properties of ideal and flawless graphene. The properties used in these articles were isotropic or orthotropic. The results of the present research show that, in addition to the size of vacancy defects, their site also significantly affects the material properties of graphene. It is observed that the

amount of temperature has a big effect on the structure getting anisotropic. In this study the effect of site and size of vacancy defects on the severity of the structure becoming anisotropic are studied by determining Lekhnitskii interaction coefficients. Unlike the molecular dynamic technique used in previous studies, which assumed a random location for vacancy defects on single-layer graphene, the present article mainly aims to systematically examine single-layer graphene sheets with a single or a series of defects. The study first finds the mechanical properties of an ideal graphene sheet using the molecular dynamic technique, and after validating the method, the effects of different sizes and numbers of vacancy defects on the mechanical properties of graphene are investigated. The results suggest that the size, site and temperature can lead to the emergence of anisotropic properties with varying intensities in graphene.

2. Molecular dynamic modelling

In the present study, the Tersoff potential energy function is used for estimation and simulation of covalent bond energy between carbon atoms in graphene. Molecular simulation is carried out with a canonical ensemble. The Velocity-Verlet algorithm is used to solve equations of motion in terms of time. The relaxation process is carried out before and after making shape changes to minimize the energy of single-layer graphene at the desired temperature. By applying strains, stress changes are calculated in terms of the applied strain, and the stiffness tensor of the material and therefore its properties are obtained. The method is first validated using the results from previous studies on defect-free graphene, and the effects of site and size of the vacancy defects on the mechanical properties of graphene are then addressed.

3. Stress-strain correlation in monolayer with desired direction

The (x, y) coordinate system can be assumed as Fig. 1. Main directions of the materials on this plane are defined with axes 1 and 2. Axis 1 makes θ angle with axis x and in line with the fibers.

The stress exerted on a coordinate can be transposed to another coordinate using transpose matrix indicated in the

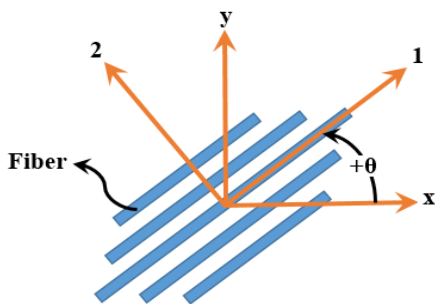


Fig. 1 The correlation between main axes of materials and the axes of the structure

following equation

$$\begin{Bmatrix} \sigma_x \\ \sigma_y \\ \tau_{xy} \end{Bmatrix} = \begin{bmatrix} C^2 & S^2 & -2CS \\ S^2 & C^2 & 2CS \\ CS & -CS & C^2 - S^2 \end{bmatrix} \begin{Bmatrix} \sigma_1 \\ \sigma_2 \\ \tau_{12} \end{Bmatrix} \quad (1)$$

$$C = \text{Cos}\theta, \quad S = \text{Sin}\theta$$

Strains can be transposed from main coordinates to geometric coordinates with a similar method. Equation (1) can be summarized as

$$\begin{Bmatrix} \sigma_x \\ \sigma_y \\ \tau_{xy} \end{Bmatrix} = [T]^{-1} \begin{Bmatrix} \sigma_1 \\ \sigma_2 \\ \tau_{12} \end{Bmatrix} \quad (2)$$

Where matrix [T] can be stated as follows

$$[T] = \begin{bmatrix} C^2 & S^2 & 2CS \\ S^2 & C^2 & -2CS \\ -CS & CS & C^2 - S^2 \end{bmatrix} \quad (3)$$

Specific orthotropic state of a monolayer is a case in which main coordinates of materials are aligned with geometric coordinates of the layer. Therefore, stress-strain correlation can be formulated as

$$\begin{Bmatrix} \sigma_x \\ \sigma_y \\ \tau_{xy} \end{Bmatrix} = \begin{Bmatrix} \sigma_1 \\ \sigma_2 \\ \tau_{12} \end{Bmatrix} = \begin{bmatrix} Q_{11} & Q_{12} & 0 \\ Q_{12} & Q_{22} & 0 \\ 0 & 0 & Q_{66} \end{bmatrix} \begin{Bmatrix} \epsilon_1 \\ \epsilon_2 \\ \gamma_{12} \end{Bmatrix} \quad (4)$$

Generally, axes are not aligned with each other. Accordingly, final stress-strain correlation in geometric coordinate should be specified based on the information of stiffness matrix in main coordinates of the materials, and its transposition to geometric coordinates. Initially, equation (4) is main coordinates and summarized as follows

$$\begin{Bmatrix} \sigma_1 \\ \sigma_2 \\ \tau_{12} \end{Bmatrix} = [Q] \begin{Bmatrix} \epsilon_1 \\ \epsilon_2 \\ \gamma_{12} \end{Bmatrix} \quad (5)$$

By considering previous equations, it can be concluded that

$$\begin{Bmatrix} \sigma_x \\ \sigma_y \\ \tau_{xy} \end{Bmatrix} = [T]^{-1} \begin{Bmatrix} \sigma_1 \\ \sigma_2 \\ \tau_{12} \end{Bmatrix} = [T]^{-1} [Q] [R] [T] [R]^{-1} \begin{Bmatrix} \epsilon_x \\ \epsilon_y \\ \gamma_{xy} \end{Bmatrix} \quad (6)$$

Expression $[R][T][R]^{-1}$ can be indicated as $[T]^{-T}$, where T stands for translation matrix. It should be taken into account that in the above-mentioned equation matrix [R] is defined as follows

$$[R] = \begin{bmatrix} 1 & 0 & 0 \\ 0 & 1 & 0 \\ 0 & 0 & 2 \end{bmatrix} \quad (7)$$

Finally, stress-strain correlation in (x, y) geometric coordinates of structure formulated as follows

$$\begin{Bmatrix} \sigma_x \\ \sigma_y \\ \tau_{xy} \end{Bmatrix} = [\bar{Q}] \begin{Bmatrix} \varepsilon_x \\ \varepsilon_y \\ \gamma_{xy} \end{Bmatrix} = \begin{bmatrix} \bar{Q}_{11} & \bar{Q}_{12} & \bar{Q}_{16} \\ \bar{Q}_{12} & \bar{Q}_{22} & \bar{Q}_{26} \\ \bar{Q}_{16} & \bar{Q}_{26} & \bar{Q}_{66} \end{bmatrix} \begin{Bmatrix} \varepsilon_x \\ \varepsilon_y \\ \gamma_{xy} \end{Bmatrix} \quad (8)$$

It should be noted that although matrix [Q⁻] may have 9 non-zero values, it has four independent and constant coefficients similar to matrix [Q]. Since properties of the layer are in orthotropic coordinates of the materials, it is called “general orthotropic layer” where the material axis of this layer does not align with geometric axis. Eq. (8) is used for layer analysis which merely includes independent constants of orthotropic materials. The advantage of using “general orthotropic layer” in comparison with anisotropic layer is that its characteristics can be easily calculated by tests. However, if the main axes of orthotropic materials are not specified, all the calculations should be carried out as an anisotropic layer. It is emphasized to use a layer with orthotropic characteristics and generalize it to a general state using Eq. (8). With a similar method, strain-stress correlation can be calculated in geometric coordinates by inverting Eq. (8).

The strain-stress correlation in main coordinates is

$$\begin{Bmatrix} \varepsilon_1 \\ \varepsilon_2 \\ \gamma_{12} \end{Bmatrix} = \begin{bmatrix} S_{11} & S_{12} & 0 \\ S_{12} & S_{22} & 0 \\ 0 & 0 & S_{66} \end{bmatrix} \begin{Bmatrix} \sigma_1 \\ \sigma_2 \\ \tau_{12} \end{Bmatrix} \quad (9)$$

Therefore, the final equation with compatibility matrix in geometric coordinates is

$$\begin{Bmatrix} \varepsilon_x \\ \varepsilon_y \\ \gamma_{xy} \end{Bmatrix} = [T]^T [S] [T] \begin{Bmatrix} \sigma_x \\ \sigma_y \\ \tau_{xy} \end{Bmatrix} = \begin{bmatrix} \bar{S}_{11} & \bar{S}_{12} & \bar{S}_{16} \\ \bar{S}_{12} & \bar{S}_{22} & \bar{S}_{26} \\ \bar{S}_{16} & \bar{S}_{26} & \bar{S}_{66} \end{bmatrix} \begin{Bmatrix} \sigma_x \\ \sigma_y \\ \tau_{xy} \end{Bmatrix} \quad (10)$$

Where [T]^T is calculated from [R][T]⁻¹[R]⁻¹.

Due to Q⁻₂₆ and Q⁻₁₆ in Eq. (8), and S⁻₂₆ and S⁻₁₆ in Eq. (10), results for general orthotropic plates will be obviously more complicated than specific orthotropic plates. By calculating some other parameters, plate analysis can be carried out in a general mode and in line with anisotropic plates. The strain-stress correlation of a desired membrane plate (anisotropic) defined as follows

$$\begin{Bmatrix} \varepsilon_1 \\ \varepsilon_2 \\ \gamma_{12} \end{Bmatrix} = \begin{bmatrix} S_{11} & S_{12} & S_{16} \\ S_{12} & S_{22} & S_{26} \\ S_{16} & S_{26} & S_{66} \end{bmatrix} \begin{Bmatrix} \sigma_1 \\ \sigma_2 \\ \tau_{12} \end{Bmatrix} \quad (11)$$

3.1 Anisotropic structure assessment using Lekhnitskii interaction coefficients

The components of the compatibility matrix of this anisotropic sheet are calculated as follows (Lekhnitskii 1963)

$$\begin{aligned} S_{11} &= 1/E_1, S_{22} = 1/E_2, \\ S_{16} &= \eta_{12,1}/E_1 = \eta_{1,12}/G_{12}, \\ S_{12} &= -\nu_{12}/E_1 = -\nu_{21}/E_2, \\ S_{26} &= \eta_{12,2}/E_2 = \eta_{2,12}/G_{12}, \\ S_{66} &= 1/G_{12} \end{aligned} \quad (12)$$

Calculating the S₁₆ and S₂₆ components requires a number of coefficients known as Lekhnitskii interaction coefficients. $\eta_{i,ij}$ is Lekhnitskii coefficient type 1, which describes stretching in the i direction due to a shearing stress in the ij plane, and equals to

$$\eta_{i,ij} = \varepsilon_i / \gamma_{ij} \quad (13)$$

In this state, $\tau_{ij} = \tau$, and all the other stresses are zero.

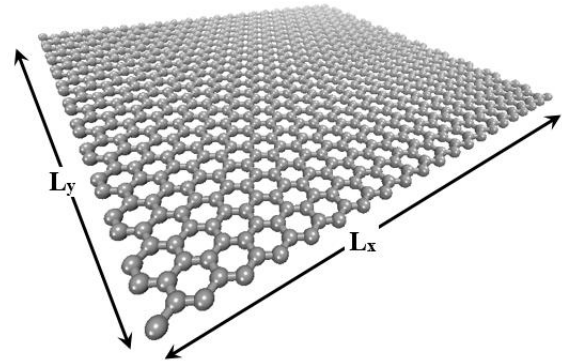


Fig. 2 the schematic representation of a flawless graphene sheet.

Table 1 A comparison of the computed mechanical properties in the present study and the ones reported in the literature

Study	Method	Young's modulus (TPa)
Present	Molecular dynamic	0.751
Lee <i>et al.</i> (2008)	Experimental	1 ± 0.1
Jiang <i>et al.</i> (2009)	Molecular dynamic	1.1
Shen <i>et al.</i> (2010)	Molecular dynamic	0.905
Ni <i>et al.</i> (2010)	Molecular dynamic	1.13
Tsai and Tu (2010)	Molecular dynamic	0.912
Kvashnin <i>et al.</i> (2010)	Molecular mechanics	1.39 (average)
Reddy <i>et al.</i> (2006)	Continuum mechanics	0.669
Liu <i>et al.</i> (2007)	Density functional theory	1.05
Sakhaee-Pour (2009)	Finite element	1.025
Georgantzinos <i>et al.</i> (2010)	Finite element	1.367
Neek-Amal and Peteers (2010)	Molecular dynamic	0.501 ± 0.032
Yanovsky <i>et al.</i> (2009)	Quantum mechanics	0.737

$\Pi_{ij,i}$ is Lekhnitskii interaction coefficient type 2, which describes shearing in the ij plane due to the normal tension applied in the i direction, and equals to

$$\eta_{ij,i} = \gamma_{ij} / \varepsilon_i \quad (14)$$

In this state, $\sigma_i = \sigma$, and all the other stresses are zero. Note that the material becomes more isotropic as the amount of Lekhnitskii coefficients approach zero, and vice versa.

4. Validating the method for defect-free single-layer graphene

In this section, the results obtained for ideal graphene compared to the results calculated in previous studies. Fig. 2 shows the schematic representation of a flawless graphene sheet. As shown in Table 1, the values of Young's modulus are fairly scattered and ranged from 0.5 TPa to 1.4 TPa. Given the present findings, the method used in the present study can clearly lead to acceptable results.

5. Problem statement

5.1 The effects of temperature on mechanical properties of single-layer graphene sheet

In this stage, the influences of temperature and also length-to-width (L_x/L_y) aspect ratio on mechanical properties of a single-layer graphene sheet are investigated. The temperature is varying from 100K to 600K and the aspect ratio is considered to change from 1.1366 to 5.5209 (Fig. 3). Figs. 4-6 show the variation of Young's (E_x , E_y) and shear modulus (G_{xy}) for single-layer graphene sheet (SLGS) with temperature ranging from 100K to 600K. It can be seen that the Young's modulus both in x and y directions strictly decrease with increases in temperature. In

contract, the shear modulus (G_{xy}) almost remains constant as temperature increases from 100K to 600K. As explained earlier, Lekhnitskii coefficients can be used for assessing the effects of site and size of vacancy defects and also temperature on the mechanical properties of graphene sheets. It is worth nothing that the mechanical properties of substances become more isotropic as the amount of Lekhnitskii coefficients approach zero, and vice versa. In this stage, the influence of temperature and aspect ratio (L_x/L_y) on the severity of the SLGS getting anisotropic are studied. To do this, the length of graphene is selected as 51.65 nm, 99.60 nm, 150.03 nm, 200.45 nm and 250.87 nm for a fixed width of 45.44 nm, i.e., the aspect ratio (L_x/L_y) are 1.1366, 2.192, 3.3017, 4.4113 and 5.5209 respectively (Fig. 3). It is observed from Figs. 7-11, in all cases with the increase of temperature the structure tends to be more anisotropic and the value of Lekhnitskii coefficient ($\Pi_{12,2}$) somehow increasing.

5.2 The effects of vacancy defects on mechanical properties of single-layer graphene sheet

Unlike the molecular dynamic technique used in previous studies, which assumed a random location for vacancy defects on single-layer graphene, the present article mainly aims to systematically examine single-layer graphene sheets with a single or a series of defects. Note that graphene sheet thickness is assumed as 3.2 nm in all the cases. Five cases are investigated for studying the effect of vacancy defects on the mechanical properties of single-layer graphene sheet as an anisotropic structure as follows:

- A single defect in the middle of the graphene sheet (Fig. 12)
- A single defect in the corner of the graphene sheet (Fig. 13)
- A double-defect at the top of the graphene sheet (Fig. 14)
- A diagonal double-defect on the graphene sheet

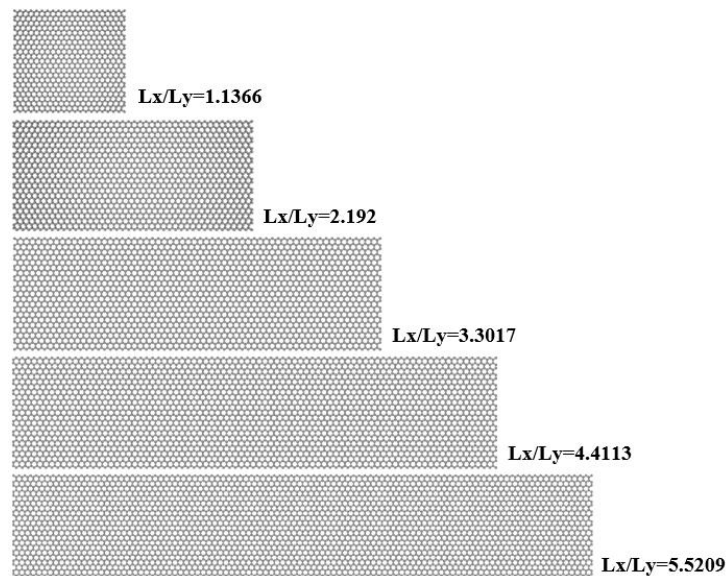


Fig. 3 The flawless graphene sheet with different aspect ratio (L_x/L_y) for a fixed width of 45.44 nm

(Fig. 15)

- A double-defect on the right side of the graphene (Fig. 16)

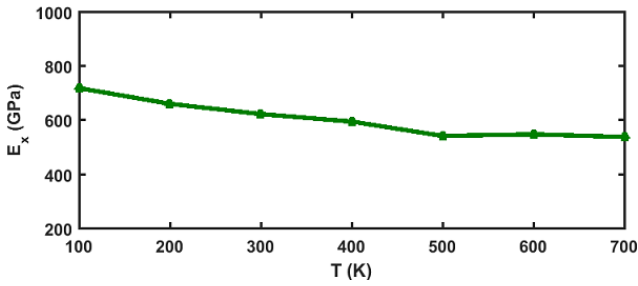


Fig. 4 The effect of temperature on Young's modulus of graphene sheet in x direction (E_x)

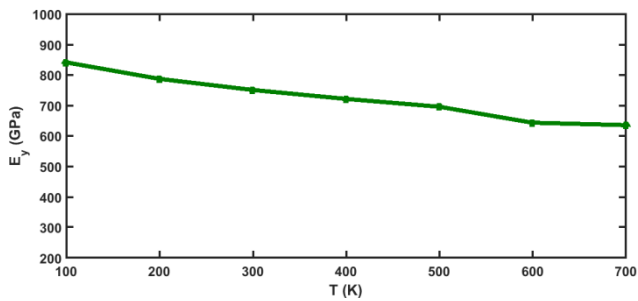


Fig. 5 The effect of temperature on Young's modulus of graphene sheet in y direction (E_y)

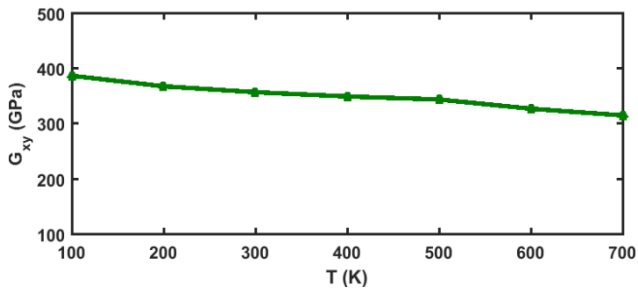


Fig. 6 The effect of temperature on shear modulus of graphene sheet (G_{xy})

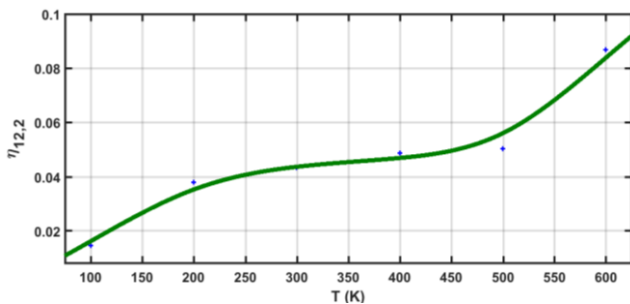


Fig. 7 The influence of temperature on the severity of the SLGS becoming anisotropic (L_x/L_y = 1.1366)

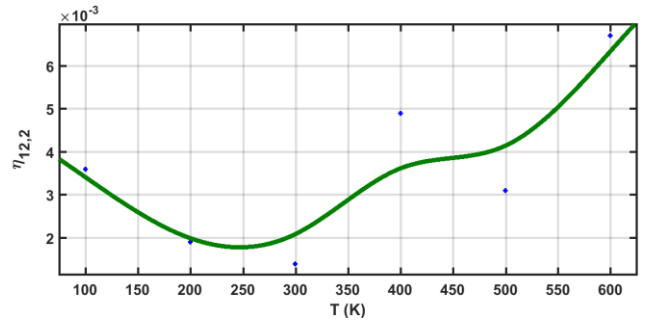


Fig. 8 The influence of temperature on the severity of the SLGS becoming anisotropic (L_x/L_y = 2.192)

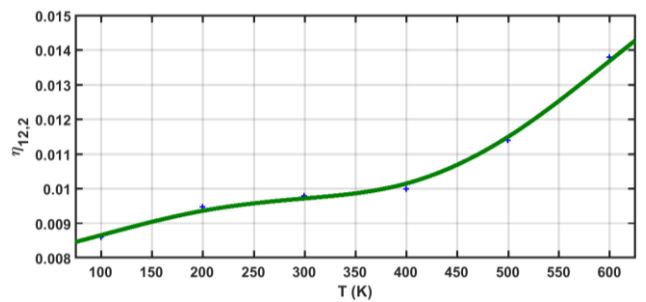


Fig. 9 The influence of temperature on the severity of the SLGS becoming anisotropic (L_x/L_y = 3.3017)

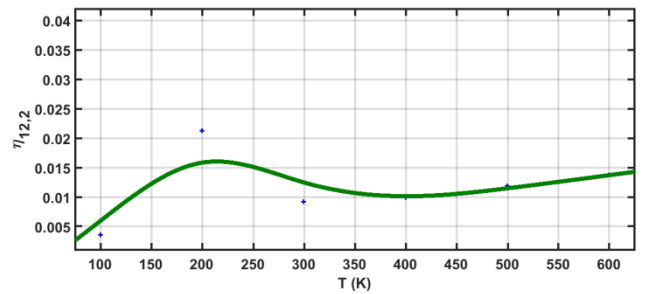


Fig. 10 The influence of temperature on the severity of the SLGS becoming anisotropic (L_x/L_y = 4.4113)

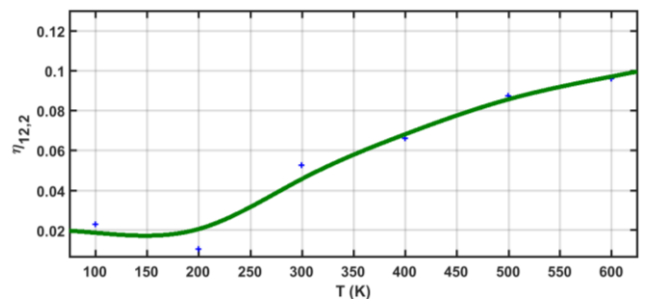


Fig. 11 The influence of temperature on the severity of the SLGS becoming anisotropic (L_x/L_y = 5.5209)

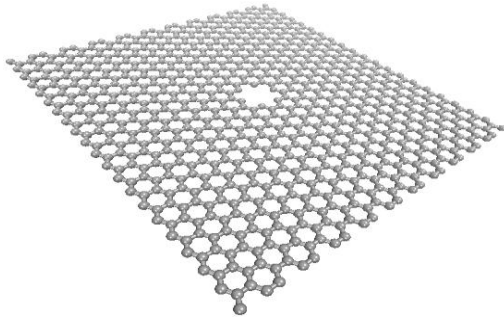


Fig. 12 Single-vacancy defect in the middle of the graphene sheet

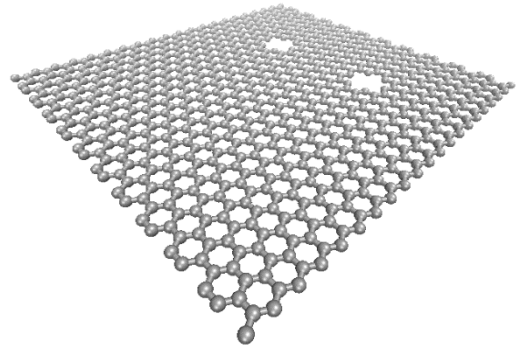


Fig. 16 Double-vacancy defect on the right-hand side of the graphene sheet

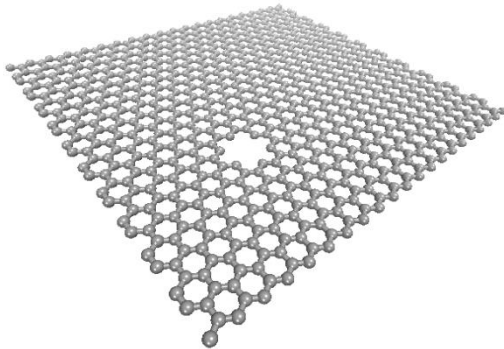


Fig. 13 Single-vacancy defect in the corner of the graphene sheet

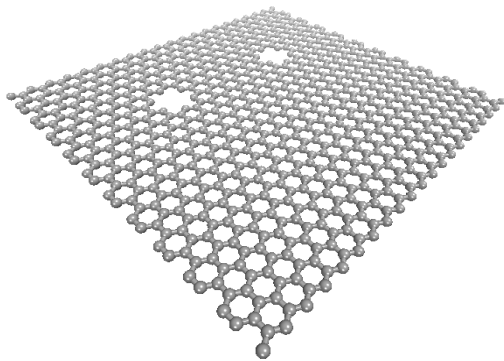


Fig. 14 Double-vacancy defect at the top of the graphene sheet

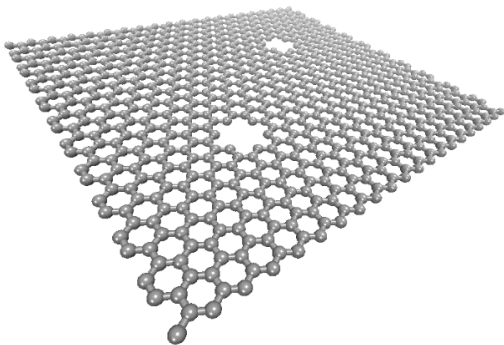


Fig. 15 Diagonal double-vacancy defect on the graphene sheet

The effects of site and size of vacancy defects on the material properties of graphene sheet in the noted cases are assessed using molecular dynamics results. The intensity of the structure becoming anisotropic can be studied in the above-mentioned cases according to the values of Lekhnitskii coefficients. The effects of different defects including single- and double vacancy defects on Young's (E_x or E_y) and shear (G_{xy}) modulus of graphene are investigated in the following. According to the Tables 2-6, in all cases, Young's and shear modulus of graphene are lower for structures with defect than those without. These material properties decrease as the size of the vacancy defect increases. It should be taken into account that the values of shear modulus is sharply decreasing in comparison with Young's modulus as the number of removed atoms increasing.

Figs. 17-21 are reported to make crystal clear the influence of defects on the material properties of single-layer graphen sheet. Given the results presented in Figs. 17

Table 2 The effect of a double-defect at the top of the graphene sheet on material properties of imperfect graphene ($L_x/L_y = 1.1366$, $T = 300K$)

Vacancy radius (nm)	E_x (GPa)	E_y (GPa)	G_{xy} (GPa)
R = 2.84	540.5514	631.8486	294.6542
R = 3.69	483.9839	549.7311	249.1723
R = 5.12	518.1459	407.4531	198.8933
R = 6.15	492.5599	276.8938	88.3804
R = 7.1	427.4211	329.9827	113.5998

Table 3 The effect of a diagonal double-defect on the material properties of imperfect graphene ($L_x/L_y = 1.1366$, $T = 300K$)

Vacancy radius (nm)	E_x (GPa)	E_y (GPa)	G_{xy} (GPa)
R = 2.84	526.6597	657.5326	342.6375
R = 3.69	458.5538	530.6295	282.2949
R = 5.12	489.3881	439.2726	256.4615
R = 6.15	357.4040	386.1099	171.5974
R = 7.1	359.2238	350.7509	159.6338

Table 4 The effect of a double-defect at the top of the graphene on the material properties of imperfect graphene ($L_x/L_y = 1.1366, T = 300K$)

Vacancy radius (nm)	E_x (GPa)	E_y (GPa)	G_{xy} (GPa)
R = 2.84	559.1481	647.4831	327.1364
R = 3.69	485.0651	581.6308	244.4673
R = 5.12	440.5191	449.8774	241.8920
R = 6.15	251.7412	377.6240	104.1642
R = 7.1	291.6378	418.6821	101.9256

Table 5 The effect of a single defect in the corner of the graphene sheet on the material properties of imperfect graphene ($L_x/L_y = 1.1366, T = 300K$)

Vacancy radius (nm)	E_x (GPa)	E_y (GPa)	G_{xy} (GPa)
R = 2.84	640.8293	608.1403	328.6012
R = 3.69	512.6069	648.7142	323.7523
R = 5.12	557.0028	654.0235	278.8591
R = 6.15	465.6993	488.6363	247.9699
R = 7.1	411.2072	448.8086	232.6059
R = 7.515	398.3045	422.7634	197.5615
R = 8.61	376.2033	439.0035	187.3168
R = 9.31	383.0660	374.7539	205.8263
R = 11.07	270.7647	323.6239	151.0142

and 18, in case of single-vacancy defects including defect in the middle and on the corner of the graphene sheets, the reduction percentage of E_x , E_y and G_{xy} sharply increasing with the increase of vacancy radius. It is worth nothing that with increasing vacancy radius, the difference between reduction percentage of E_x and E_y somehow reduced.

In case of double-vacancy defects (Figs. 19-21) including double-vacancy defect at the top, at the right side of graphene and diagonal double-vacancy defect in the graphene, the reduction percentage of E_x and E_y increasing

Table 6 The effect of a single defect in the middle of the graphene sheet on the material properties of imperfect graphene ($L_x/L_y = 1.1366, T = 300K$)

Vacancy radius (nm)	E_x (GPa)	E_y (GPa)	G_{xy} (GPa)
R = 2.84	691.3710	540.9188	363.2081
R = 3.69	540.3232	629.0517	288.0268
R = 5.12	539.7213	660.3958	289.1454
R = 6.15	505.8598	508.5937	271.7107
R = 7.1	500.9569	508.1838	240.1680
R = 7.515	405.6374	357.6737	201.0596
R = 8.61	413.8241	426.6777	197.0534
R = 9.31	343.4435	444.1128	195.5815
R = 11.07	360.3825	401.9742	112.0520
R = 11.36	400.9142	362.4770	98.9211
R = 11.625	275.3987	323.5803	131.2298
R = 12.38	286.8114	219.4155	110.6566
R = 13.525	168.3484	303.1303	79.6161
R = 14.825	206.6496	202.6409	28.5830
R = 15.62	147.2413	176.7330	37.4021

with the increase of vacancy radius. It should be taken into account that with the increase of vacancy radius, the rate of reduction of E_x gets much more than E_y in graphene with double-vacancy defect at the top contrary to graphene with defects at the right or left side. Figs. 17-21 show somehow that the rate of reduction of G_{xy} is much more than the Young's modulus reduction in the x and y directions.

6. Conclusions

The effects of size and site of vacancy defects on the material properties of the graphene using the molecular dynamic method and equations related to lekhmitskii interaction coefficients are investigated in this study. The influences of temperature and also length-to-width (L_x/L_y)

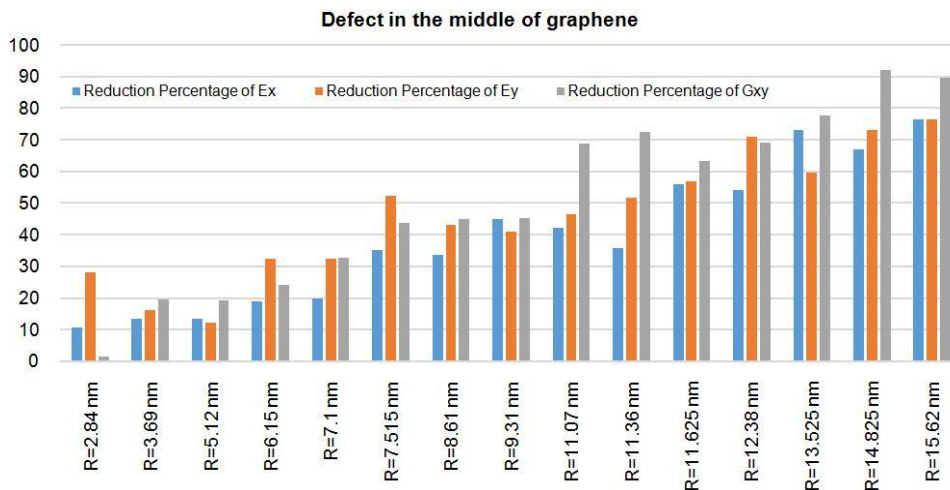


Fig. 17 The effect of single-vacancy defect in the middle of graphene on the Young's and shear modulus ($L_x/L_y = 1.1366, T = 300K$)

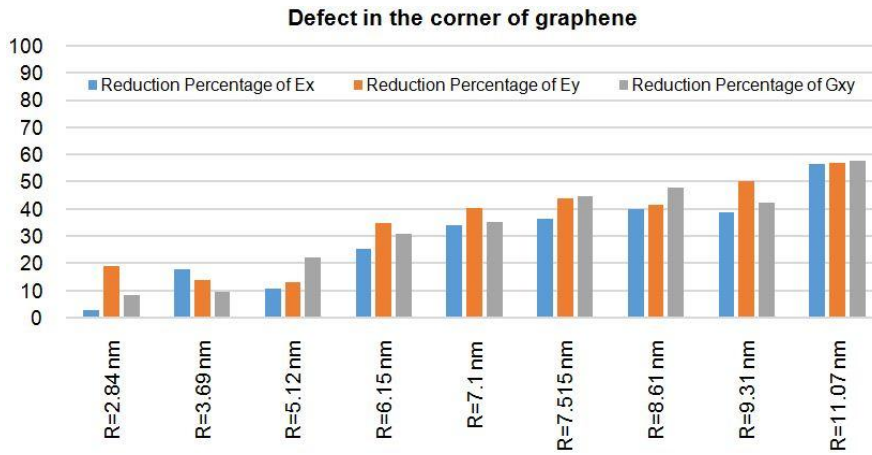


Fig. 18 The effect of single-vacancy defect in the corner of graphene on the Young's and shear modulus ($L_x/L_y = 1.1366$, $T = 300K$)

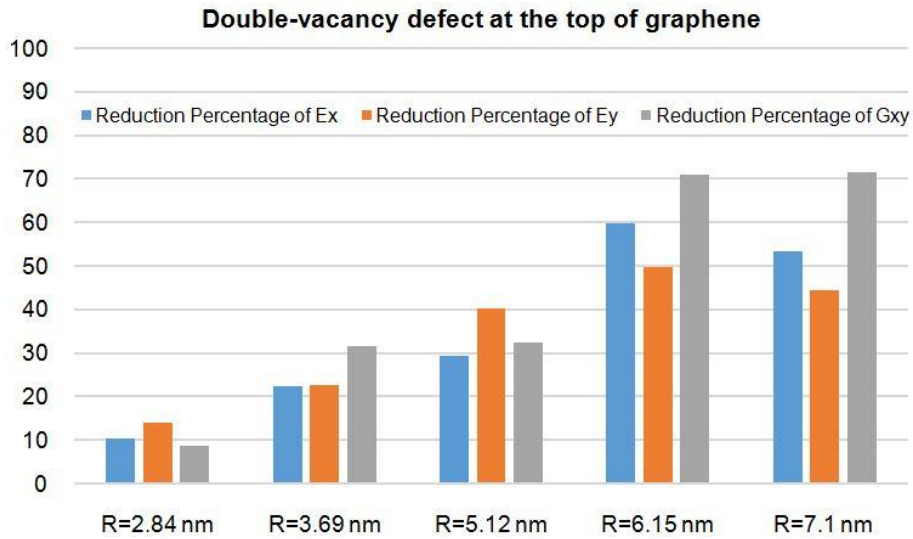


Fig. 19 The effect of double-vacancy defect at the top of graphene on the Young's and shear modulus ($L_x/L_y = 1.1366$, $T = 300K$)

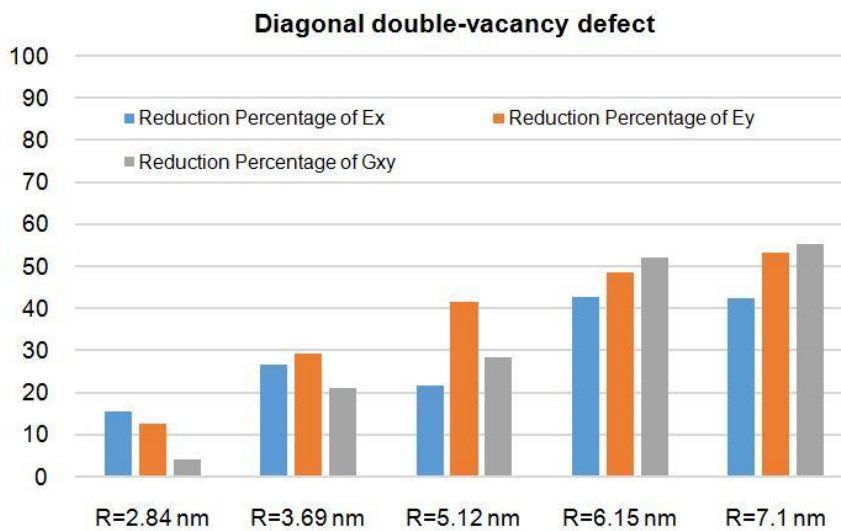


Fig. 20 The effect of diagonal double-vacancy defect on the Young's and shear modulus ($L_x/L_y = 1.1366$, $T = 300K$)

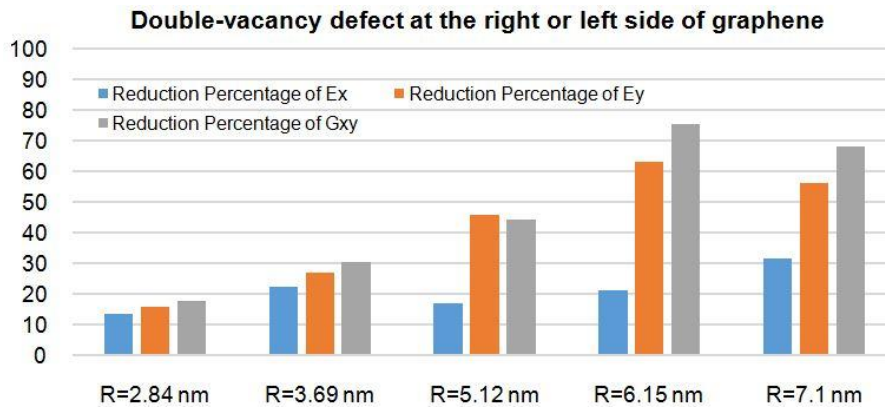


Fig. 21 The effect of double-vacancy defect at the right or left side of graphene on the Young's and shear modulus ($L_x/L_y = 1.1366$, $T = 300K$)

aspect ratio on mechanical properties of a single-layer graphene sheet are investigated. In the present study, the temperature is varying from 100K to 600K and the aspect ratio is considered to change from 1.1366 to 5.5209. The main purpose of this research is to clarify how imperfect graphene has anisotropic properties in certain conditions and using the properties of ideal graphene for imperfect graphene will cause erroneous results. According to the present study, using material properties of flawless graphene for imperfect structure can lead to inaccurate results. From this study some conclusions can be made as following:

- The Lekhnitskii interaction coefficients somehow increase with the increase of vacancy radius and the material properties of the structure show greater tendency to become anisotropic.
- In all cases with the increase of temperature, the structure tends to be more anisotropic and the value of parameter $\Pi_{12,2}$ somehow increasing.
- It can be seen that the Young's modulus both in x and y directions strictly decrease with increases in temperature. In contract, the shear modulus (G_{xy}) almost remains constant as temperature increases from 100K to 600K.
- In all cases, Young's and shear modulus of graphene are lower for structures with defect than those without. These material properties decrease as the size of the vacancy defect increases.
- It should be taken into account that the value of shear modulus is sharply decreasing in comparison with Young's modulus as the number of removed atoms increasing.
- Given the results presented in this study, in case of single-vacancy defects including defect in the middle and on the corner of the graphene sheets, the reduction percentage of E_x , E_y and G_{xy} sharply increasing with the increase of vacancy radius. It is worth nothing that with increasing vacancy radius, the difference between reduction percentage of E_x and E_y somehow reduced.
- In case of double-vacancy defects including double-vacancy defect at the top, at the right or left side of

graphene and diagonal double-vacancy defect in the graphene, the reduction percentage of E_x and E_y increasing with the increase of vacancy radius.

It should be taken into account that with the increase of vacancy radius, the rate of reduction of E_x gets much more than E_y in graphene with double-vacancy defect at the top contrary to graphene with double-vacancy defect at the right side.

References

- Allahkarami, F., Nikkhah-bahrami, M. and Ghassabzadeh Saryazdi, M. (2017), "Damping and vibration analysis of viscoelastic curved microbeam reinforced with FG-CNTs resting on viscoelastic medium using strain gradient theory and DQM", *Steel Compos. Struct., Int. J.*, **25**(2), 141-155.
- Allahkarami, F., Nikkhah-bahrami, M. and Ghassabzadeh Saryazdi, M. (2018), "Nonlinear forced vibration of FG-CNTs-reinforced curved microbeam based on strain gradient theory considering out-of-plane motion", *Steel Compos. Struct., Int. J.*, **26**(6), 673-691.
- Bu, H., Chen, Y., Zou, M., Yi, H., Bi, K. and Ni, Z. (2009), "Atomistic simulations of mechanical properties of graphene nanoribbons", *Phys. Lett. A*, **373**(37), 3359-3362.
- Dai, H. (2002), "Carbon Nanotubes: Synthesis, Integration, and Properties", *Acc. Chem. Res.*, **35**(12), 1035-1044.
- Georgantzinos, S.K., Giannopoulos, G.I. and Anifantis, N.K. (2010), "Numerical investigation of elastic mechanical properties of graphene structures", *Mater. Des.*, **31**(10), 4646-4654.
- Iijima, S. (1991), "Helical microtubules of graphitic carbon", *Nature*, **354**, 56-58.
- Jalali, S.K., Jomehzadeh, E. and Pugno, N.M. (2016), "Influence of out-of-plane defects on vibration analysis of graphene: Molecular Dynamics and Non-local Elasticity approaches", *Superlattices Microstruct.*, **91**, 331-344.
- Jiang, J.W., Wang, J.S. and Li, B. (2009), "Young's modulus of graphene: A molecular dynamics study", *Phys. Rev. B*, **80**(11), 113405-113408.
- Kumar, D. and Srivastava, A. (2016), "Elastic properties of CNT- and graphene-reinforced nanocomposites using RVE", *Steel Compos. Struct., Int. J.*, **21**(5), 1085-1103.
- Kvashnin, A.G., Sorokin, P.B., Kvashnin, D.G. (2010), "The Theoretical Study of Mechanical Properties of Graphene Membranes", *Fuller. Nanotubes Carbon Nanostruct.*, **18**(4-6),

- 497-500.
- Lee, C., Wei, X.D., Kysar, J.W. and Hone, J. (2008), "Measurement of the elastic properties and intrinsic strength of monolayer graphene", *Science*, **321**(5887), 385-388.
- Lekhnitskii, S.G. (1963), "Theory of elasticity of an anisotropic elastic body", *Phys. Today*, **17**, 84 p.
- Liu, F., Ming, P. and Li, J. (2007), "Ab initio calculation of ideal strength and phonon instability of graphene under tension", *Phys. Rev. B*, **76**(6), 064120-064127.
- Ma, J., Alfè, D., Michaelides, A. and Wang, E. (2009), "Stone-Wales defects in graphene and other planar sp²-bonded materials", *Phys. Rev. B*, **80**, 1-4.
- Marin, M. (1997), "Cesaro means in thermoelasticity of dipolar bodies", *Acta Mechanica*, **122**(1-4), 155-168.
- Marin, M. (2008), "Weak Solutions in Elasticity of Dipolar Porous Materials", *Math. Probl. Eng.*, 1-8.
DOI: <http://dx.doi.org/10.1155/2008/158908>
- Marin, M. (2010), "Some estimates on vibrations in thermoelasticity of dipolar bodies", *J. Vib. Control*, **16**(1), 33-47.
- Marin, M. (2016), "An approach of a heat-flux dependent theory for micropolar porous media", *Meccanica*, **51**(5), 1127-1133.
- Marin, M. and Ōchsner, A. (2017), "The effect of a dipolar structure on the Holder stability in Green-Naghdi thermoelasticity", *Continu. Mech. Thermodyn.*, **29**(6), 1365-1374.
- Moradi-Dastjerdi, R. and Momeni-Khabisi, H. (2016), "Dynamic analysis of functionally graded nanocomposite plates reinforced by wavy carbon nanotube", *Steel Compos. Struct., Int. J.*, **22**(2), 277-299.
- Moradi-Dastjerdi, R. and Payganeh, G. (2017a), "Thermoelastic dynamic analysis of wavy carbon nanotube reinforced cylinders under thermal loads", *Steel Compos. Struct., Int. J.*, **25**(3), 315-326.
- Moradi-Dastjerdi, R. and Payganeh, G. (2017b), "Transient heat transfer analysis of functionally graded CNT reinforced cylinders with various boundary conditions", *Steel Compos. Struct., Int. J.*, **24**(3), 359-367.
- Navarro, C.G., Weitz, R.T., Bittner, A.M., Scolari, M., Mews, A., Burghard, M. and Kern, K. (2007), "Electronic transport properties of individual chemically reduced graphene oxide sheets", *Nano Lett.*, **7**(11), 3499-3503.
- Neek-Amal, M. and Peeters, F.M. (2010), "Linear reduction of stiffness and vibration frequencies in defected circular monolayer graphene", *Phys. Rev. B*, **81**(23), 235437.
- Ni, Z., Bu, H., Zou, M., Yi, H., Bi, K. and Chen, Y. (2010), "Anisotropic mechanical properties of graphene sheets from molecular dynamics", *Physica B*, **405**(5), 1301-1306.
- Reddy, J.N. (2004), *Mechanics of Laminated Composite Plates and Shells-Theory and Analysis*, (Second Edition), CRC Press.
- Reddy, C.D., Rajendran, S. and Liew, K.M. (2006), "Equilibrium configuration and continuum elastic properties of finite sized graphene", *Nanotechnology*, **17**(3), 864-870.
- Sakhaee-Pour, A. (2009), "Elastic properties of single-layered graphene sheet", *Solid State Commun.*, **149**(1), 91-95.
- Shen, L., Shen, H.S. and Zhang, C.L. (2010), "Temperature-dependent elastic properties of single layer graphene sheets", *Mater. Des.*, **31**, 4445-4449.
- Soleimani, A., Naei, M.H. and Mosavi Mashhadi, M. (2017), "Nonlocal postbuckling analysis of graphene sheets with initial imperfection based on first order shear deformation theory", *Results in Phys.*, **7**, 1299-1307.
- Stankovich, S., Dikin, D.A., Dommett, G.H., Kohlhaas, K.M., Zimney, E.J., Stach, E.A., Piner, R.D., Nguyen, S.T. and Ruoff, R.S. (2006), "Graphene-based composite materials", *Nature*, **442**(7100), 282-286.
- Sun, X., Fu, Z. and Xia, M. (2014), "Effects of vacancy defect on the tensile behavior of graphene", *Theor. Appl. Mech. Lett.*, **4**(5), 51002.
- Sun, X.Y., Hu, H., Caob, C. and Xua, Y.J. (2015), "Anisotropic vacancy-defect-induced fracture strength loss of graphene", *RSC Adv.*, **5**(2), 13623-13627.
- Tahouneh, V. (2016), "Using an equivalent continuum model for 3D dynamic analysis of nanocomposite plates", *Steel Compos. Struct., Int. J.*, **20**(3), 623-649.
- Tahouneh, V. (2017), "Effects of CNTs waviness and aspect ratio on vibrational response of FG-sector plate", *Steel Compos. Struct., Int. J.*, **25**(6), 649-661.
- Tahouneh, V., Mosavi Mashhadi, M. and Naei, M.H. (2016), "Finite element and micromechanical modeling for investigating effective material properties of polymer-matrix nanocomposites with microfiber, reinforced by CNT arrays", *Int. J. Adv. Struct. Eng.*, **8**(3), 297-306.
- Tornabene, F., Fantuzzi, N., Ubertini, F. and Viola, E. (2015), "Strong formulation finite element method based on differential quadrature: a survey", *Appl. Mech. Rev.*, **67**(2), 1-55.
- Tornabene, F., Baccocchi, M., Fantuzzi, N. and Reddy, J.N. (2018), "Multiscale approach for three-phase CNT/polymer/fiber laminated nanocomposite structures", *Polym. Compos.* [In Press] DOI: 10.1002/pc.24520
- Tsai, J.L. and Tu, J.F. (2010), "Characterizing mechanical properties of graphite using molecular dynamics simulation", *Mater. Des.*, **31**(1), 194-199.
- Udupa, A. and Martini, A. (2011), "Model predictions of shear strain-induced ridge defects in graphene", *Carbon*, **49**(11), 3571-3578.
- Wu, Y., Yin, J., Xie, W., Zhang, W., Wu, B., Jiang, Y. and Zhang, P. (2015), "Effect of vacancy distribution on the relaxation properties of graphene: A molecular dynamics study", *IET Micro. Nano Lett.*, **10**(12), 693-695.
- Xie, G., Shen, Y., Wei, X., Yang, L., Xiao, H., Zhong, J. and Zhang, G. (2014), "A bond-order theory on the phonon scattering by vacancies in two-dimensional materials", *Electron. Spintron. devices*, 1-23.
- Yakobson, B.I., Brabec, C.J. and Bernholc, J. (1996), "Nanomechanics of Carbon Tubes: Instabilities beyond Linear Response", *Phys. Rev. Lett.*, **76**, 2511-2514.
- Yanovsky, Y.G., Nikitina, E.A., Karnet, Y.N. and Nikitin, S.M. (2009), "Quantum Mechanics Study of the Mechanism of Deformation and Fracture of Graphene", *Phys. Mesomech.*, **12**, 254-262.
- Zhang, Y., Chen, Y., Zhou, K. and Liu, C. (2009), "Improving gas sensing properties of graphene by introducing dopants and defects: a first-principles study", *Nanotechnology*, **20**(18), 185504.